UNIVERSITÀ DEGLI STUDI DI PADOVA

Dipartimento di Fisica e Astronomia "Galileo Galilei"

Corso di Laurea in Fisica

Tesi di Laurea

Measurement of B_s^0 meson lifetime in the $B_s^0 \to J/\psi\phi$ decay channel at CMS experiment.

Relatore

Prof. Paolo Ronchese

Laureando

Alessandro Valente

Anno Accademico 2018/2019

Contents

Chapter 1

Introduction

The physics of B-meson offers a wide field, at the TeV energy scale, of opportunities in the search for New Physics and in the Standard Model tests.
The decay of mesons due to weak interaction may violate the product of charge-conjugation and parity symmetry (CP) stating the invariance of the system under mirror inversion of its coordinate system and particle-antiparticle interchange; this effect is called "direct CP violation".

The mass eigenstates of the B_s^0 meson are neither flavour eigenstates, leading to a phenomenon known as flavor oscillation, nor CP eigenstates leading to a CP violation called "mixing induced violation". The interference between the direct violation and the mixing induced violation leads to the appearance of a phase ϕ_s.

Important tests of the Standard Model are given by the measurement of those quantities[1]:

- the weak phase ϕ_s,
- light and heavy B_s^0 mass eigenstates decay width difference $\Delta\Gamma_s$.

The correct estimation of those quantities requires a high precision during the measurement and the analysis process due to the small difference between light and heavy mass and between short and long decay time; particular attention is required in the reconstruction of the B_s^0 creation and decay point.

The goal of this thesis is the estimation of the systematic effects depending on the measurement of the B_s^0 creation point; this is done studying the B_s^0 lifetime which is highly affected by those effects. The study was performed considering the decay channel $B_s^0 \to J/\psi\phi$, followed by the cascade decays $J/\psi \to \mu^+\mu^-$ and $\phi \to K^+K^-$.

The analysis method is divided in three steps: in the first step the B_s^0 decays are reconstructed from the tracks of the decay products and filtered applying a set of selection cuts, in the next step the position of the B_s^0 creation point is estimated and its flight

distance is computed, the final step consists in a fit procedure to estimate the B_s^0 mean lifetime.

The analysis was performed using data collected in 2018 at a collision energy of $\sqrt{s} = 13$ TeV, a sample of Monte Carlo events, simulated with PYTHIA[2] and EVTGEN[3], was also used.

Chapter 2

The CMS experiment

The CMS (Compact Muon Solenoid) experiment[4] is a detector operating at the Large Hadron Collider at CERN designed for high-energy collision analysis.

The detector is composed by several detection layers with cylindrical symmetry around the beam axis: the inner layer is the Pixel Detector, followed by the Silcon Tracker, the Calorimeters (ECAL and HCAL), the Superconducting Solenoid and, in the outermost part, the Muon Detectors, as shown in **Figure 2.1**:

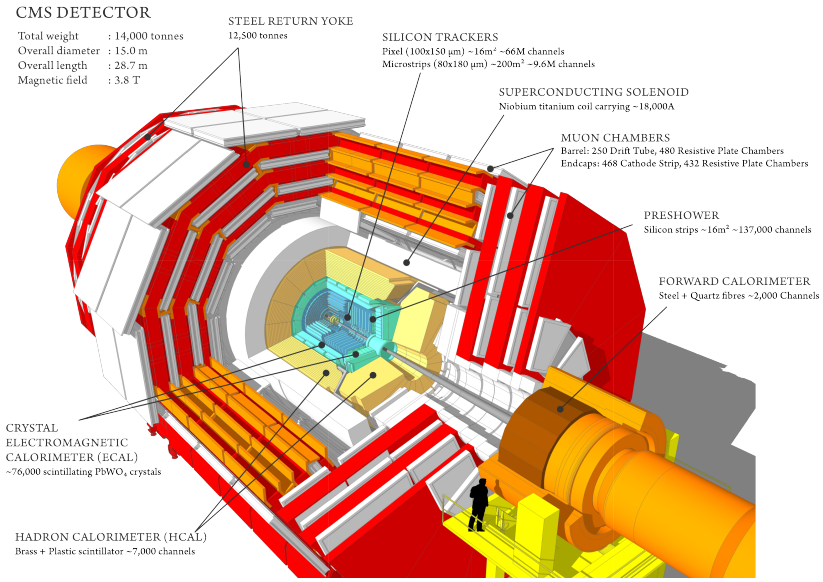

Figure 2.1: CMS detector layers

The cartesian coordinate system has the z-axis along the beam, in the counter clockwise direction, the x-axis pointing at the center of the collider ring and the y-axis in the vertical direction pointing upward.

Particles momentum is usually expressed using a polar coordinate system composed by the p_T, defined as the module of the momentum projection on the XY-plane, the azimuthal angle ϕ defined in the XY-plane starting from the x-axis, and the pseudorapidity, defined as $\eta = -\log[\tan(\theta/2)]$ where θ is the polar angle, referred to the z-axis.

The particles generated from the beam collisions are bent by the magnetic field generated from the Superconducting Solenoid: the solenoid provides an uniform axial magnetic field over 12.5m of length with a 3.15m of free-bore radius and an intensity of 3.8T; being positioned after the calorimeter the number of particles showering before the calorimeters themselves is minimized improving the particle reconstruction. The typical particle path inside the detector is shown in **Figure 2.2**:

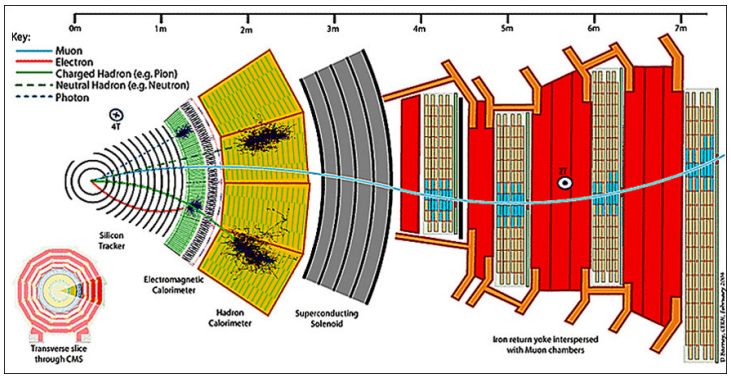

Figure 2.2: Typical path of a particle in the CMS detector

1 Tracker

At CMS the tracking system is composed by the Pixel Detector and the Strip Detector both composed by many subsystems. The whole tracker is made of silicon with sensors placed in a radial symmetry along the interaction region.

The system is designed to provide high resolution for particles up to pseudorapidity of $|\eta| < 2.4$; the high precision is essential to reconstruct, starting from the bent trajectories of the charged particles, the particle momenta and the coordinates of primary and secondary vertices.
The tracker layout is shown is **Figure 2.3**:

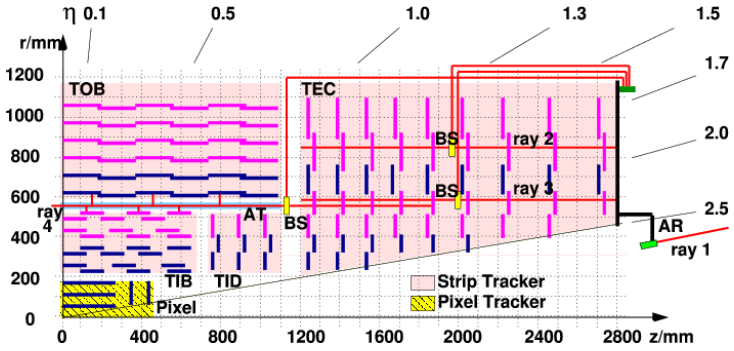

Figure 2.3: Layout of the tracker system at CMS

2 Calorimeters

The CMS calorimeter system, shown in **Figure 2.4**, is composed by two concentric calorimeters: the inner one (ECAL) is an electromagnetic calorimeter while the outer one (HCAL) is an hadron calorimeter.

ECAL is an homogeneous calorimeter composed of lead tungstenate which has both absorber and sensitive function, the material was chosen due to its fast response besides having a small Moliere radius and short radiation length.

HCAL is composed of four parts: the Barrel (HB), the End-cap (HE), an Outer calorimeter (HO) and a Foward calorimeter (HF).
HB and HE are sample calorimeters using plastic scintillator and brass as active and absorber material.
HF collects Cherenkov radiation emitted from the components of the electromagnetic shower.
HO helps the muons identification and works as tail-catcher of the hadronic showers.

3 Muon chambers

The muon system at CMS, shown in **Figure 2.5**, is composed by three detectors able to cover the region up to a pseudorapidity value of $|\eta| < 2.4$.

The Drift Tubes (DT) are used in the barrel region due to the low rate of muons, a small background induced from neutrons and an uniform magnetic field mostly contained in the solenoid; there are four stations of DT among the layers covering the pseudorapidity region of $|\eta| < 1.2$.

The Cathode Strip Chambers (CSC) are used in the end-cap regions due to the high level of background, as well as the muon rate, besides the non-uniform magnetic field; CSC covers the pseudorapidity region of $0.9 < |\eta| < 2.4$.

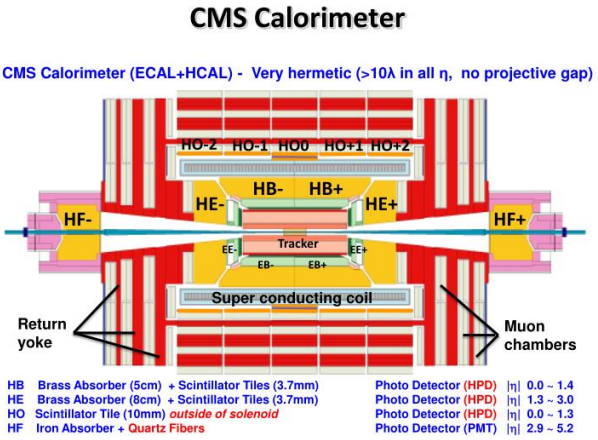

Figure 2.4: Layout of the calorimeters at CMS

The Resistive Plate Chambers (RPC) are placed in both regions, the RPC function is providing a dedicated, independent and fast trigger system; RPC covers the pseudorapidity region of $|\eta| < 1.6$.

The whole system is able to complete the tasks of muon identification and momentum measurement while triggering the reconstructed particles; during this process muons may be classified in three categories:

- Stand-alone: the reconstruction has been performed using only the data collected from the muon detectors,
- Global: the reconstruction is performed starting from the muon segment data adding the tracker data afterwards,
- Tracker: the reconstruction is performed using the tracks of the inner layer and comparing the results with the calorimeter and muon system expected data.

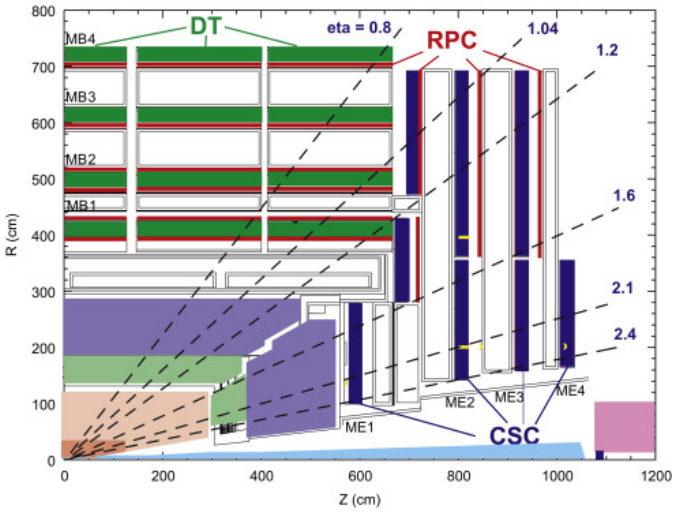

Figure 2.5: Layout of the muon system at CMS

4 Trigger

At LHC designed luminosity around 10^9 collisions per second happens, due to the storage capacity it was necessary to implement a trigger system able to reject a high number of events, reducing their number by 7 orders of magnitude. At CMS the first part of the trigger system consists in a Level-1 trigger based on dedicated electronics, which is designed to have an optimal output rate, accepting events of the type selected for the analysis through the information obtained from the calorimeter and the detectors. After the L1 trigger there is an array of High-Level Triggers (HLT) which are software-based triggers that filter the events while reconstructing specific objects.[5]

Chapter 3

Particle Reconstruction

The analysis has been performed using data collected during 2018, period "D", by the CMS experiment, corresponding to an integrated luminosity of $\mathcal{L} = 8.04$ fb^{-1}, a sample of 10^8 Monte Carlo $B_s^0 \to J/\psi\phi$ events, simulated with PYTHIA[2] and EVTGEN[3], was also used.

The analyzed data sample includes events accepted by an HLT trigger ("Displaced Trigger" in the following) that requires two muons with a transverse momentum $p_T > 4$ GeV/c and an invariant mass $2.9 < m < 3.3$ GeV/c^2 compatible with being generated from a common vertex, displaced from the interaction point with a distance significance $L/\sigma_L > 3$; it also requires the presence of two additional tracks with $p_T > 0.8$ GeV/c and invariant mass $0.95 < m < 1.3$ GeV/c^2, in the assumption that the particles are kaons, the tracks are then fitted to a common vertex with low quality requirements.

The results have been compared with the ones obtained with another HLT ("Additional Muon Trigger" in the following) which also requires a muon pair with transverse momentum $p_T > 4$ GeV/c and an invariant mass $2.9 < m < 3.3$ GeV/c^2, plus an additional muon with $p_T > 2$ GeV/c; the additional muon is required because B-hadrons are usually created in pairs, from the hadronization of $b\bar{b}$ quark pairs, and a fraction of the created B-hadrons decays in channels having a muon in the final state.

A more inclusive inclusive trigger generically requiring a charmonium decaying to $\mu^+\mu^-$ ("Inclusive trigger" in the following) was also used.

1 J/ψ reconstruction

The reconstruction of the J/ψ is done considering all the opposite sign muon pairs in the event with both muons having a transverse momentum $p_T(\mu^\pm) > 2.0$ GeV/c: using the tracks momentum and energy the invariant mass of the particle is reconstructed and the decay point is estimated fitting the tracks to a common vertex.

In **Figure 3.1** the histogram of the reconstructed J/ψ mass is shown:

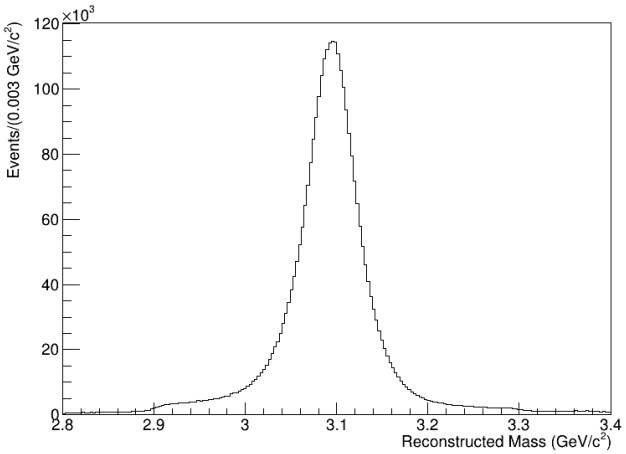

Figure 3.1: $J/\psi \to \mu^+\mu^-$ reconstructed mass

2 ϕ reconstruction

In the same way as the J/ψ the ϕ candidate is obtained from a pair of particles, assumed to be kaons, both having a $p_T(K^{\pm}) > 0.7$ GeV/c, whose tracks are fitted to a common vertex; from the tracks energy and momentum the ϕ invariant mass is then computed.

In **Figure 3.2** the histogram of the reconstructed ϕ mass is shown:

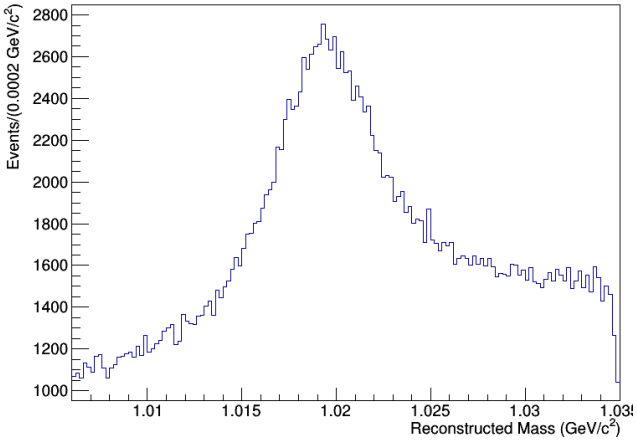

Figure 3.2: $\phi \to K^+K^-$ reconstructed mass

3 B_s^0 reconstruction

Using the tracks from the J/ψ and ϕ candidates the B_s^0 is reconstructed; J/ψ candidates are accepted if having $|m_{\mu\mu} - m_{PDG}(J/\psi)| < 0.150$ GeV/c^2 and ϕ candidates are required to have $|m_{KK} - m_{PDG}(\phi)| < 0.010$ GeV/c^2, where the world average mass values have been used[6]: $m_{J/\psi} = 3096.916 \pm 0.011$ MeV/c^2 and $m_\phi = 1019.461 \pm 0.019$ MeV/c^2.

The B_s^0 mass was obtained from a kinematic fit where the muon pair invariant mass was constrained at the J/ψ mass PDG value.

The position of the B_s^0 decay point, also called secondary vertex (SV in the following), is then estimated fitting the tracks to a common vertex, since the flight distance of the J/ψ and ϕ are negligible due to their extremely short lifetime, the chi square probability of the common vertex is required to be $prob(\chi^2) > 0.02$.

To have a better signal to background ratio additional cuts have been applied to particles transverse momentum and pseudorapidity. The full selection is summarized in **Table 3.1**.

In **Figure 3.3** the B_s^0 reconstructed mass distribution, obtained with the "Inclusive" trigger, is shown:

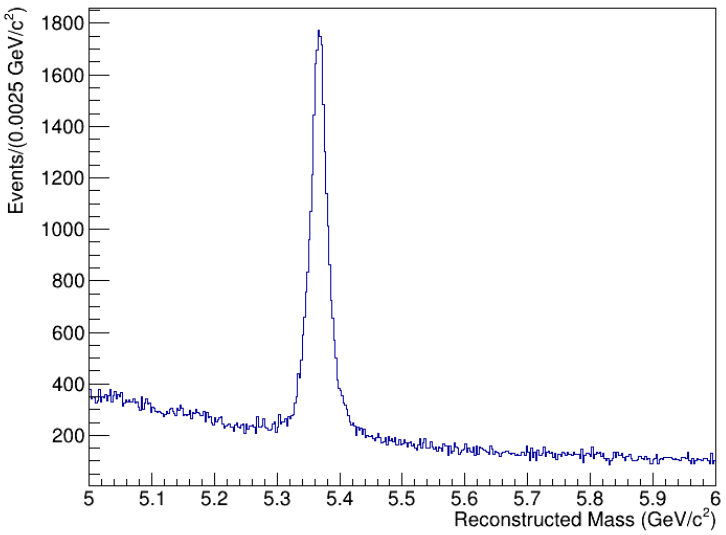

Figure 3.3: B_s^0 reconstructed mass from "Inclusive" trigger data sample

J/ψ requirements	$p_T(J/\psi) > 8.0\,\mathrm{GeV}$ $p_T(\mu^{\pm}) > 4.0\,\mathrm{GeV}$ $\lvert M(J/\psi) - M_{PDG}(J/\psi)\rvert < 0.150\,\mathrm{GeV/c^2}$ $\lvert\eta(\mu^{\pm})\rvert < 2.2$
ϕ requirements	$p_T(K^{\pm}) > 1.2\,\mathrm{GeV}$ $\lvert M(\phi) - M_{PDG}(\phi)\rvert < 0.010\,\mathrm{GeV/c^2}$
B_s^0 requirements	$p_T(B_s^0) > 27.0\,GeV/c$ Vertex Probability $> 10\%$

Table 3.1: Cuts applied in the $B_s^0 \rightarrow J/\psi\phi$ reconstruction

4 Trigger selection

The histograms previously shown are produced using the data sample obtained from the "Inclusive" trigger, in the following analysis also the "Displaced" and/or "Additional Muon" trigger have been used.

Using a data set obtained from a sample of 10^8 Monte Carlo simulated events, it's possible to obtain some information about the acceptance and efficiency of the triggers.

In **Table 3.2** the results are shown: it's important to observe that the "Additional Muon" trigger is passed by a very low percentage of events while the "Displaced" one is passed by a number of event that remains on the same order of magnitude of the previously selected events.

Event	Number of events ($*10^6$)	Fraction
Selected events	7.78	1
Displaced trigger	4.09	0.527
Additional muon trigger	0.025	0.003
Logic OR of triggers	4.11	0.528

Table 3.2: Number of events passing the trigger on MC simulated data: the "selected" events are the ones that passed the cuts described in the previous section while the fraction refers to the ratio of selected events that passed also the trigger selection

For this reason the "Additional Muon" trigger is not used alone; 3 different data samples will then be considered in the following analysis:

- Data sample with events selected by the "Inclusive" trigger,
- Data sample with events selected by the "Displaced" trigger,
- Data sample with events selected by the Logic OR combination of the "Displaced" and "Additional Muon" triggers ("OR trigger" in the following).

The reconstructed mass distributions of the B_s^0 obtained from these data samples are shown in **Figure 3.4** while in **Table 3.3** the numbers of events belonging to each data sample are reported:

Selection	Events
Inclusive trigger	183704
Displaced trigger	60603
OR trigger	72199

Table 3.3: Number of reconstructed and selected events with the used triggers

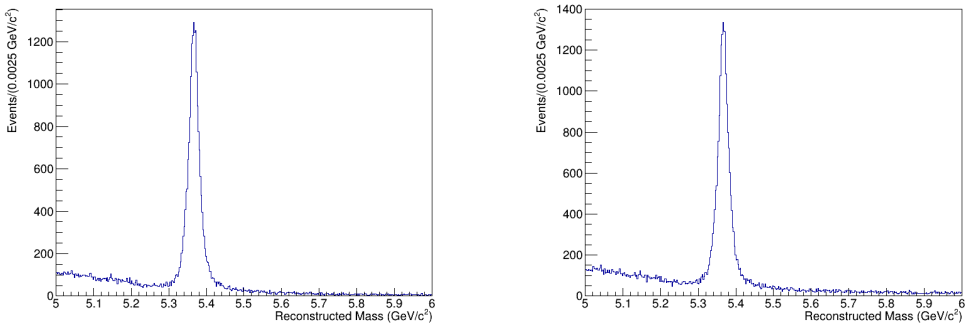

(a) "Displaced" trigger (b) "OR" trigger

Figure 3.4: B_s^0 reconstructed mass obtained from different data samples

Comparing with **Figure 3.3** it's easy noticed that the level of background is significantly reduced. That's due to the presence, in the "Inclusive" trigger, of a large fraction of J/ψ events not coming from the decay of B-hadrons, which can be paired with other particles and randomly mimic a B_s^0 decay.

Chapter 4

Flight Distance

The flight distance is estimated from the measured points of the B_s^0 creation and decay. The decay point is given by the SV position, obtained as described before, while the creation point is assumed to be the proton-proton interaction point.

In pp collision at high energy a lot of particles are produced, giving several tracks coming from a common point, named "Primary Vertex" (PV in the following).
The position of the primary vertex can be estimated by fitting the tracks in the same way as it's done for the SV; at LHC the situation is complicated by the very high luminosity leading to the presence of many collision points and, as a consequence, many primary vertices.

1 Primary vertex reconstruction

In the CMS analysis software primary vertices are reconstructed in the standard data processing; at LHC luminosities a few tens of primary vertices are reconstructed in each event. During 2018 the average number of primary vertices was around 30, with a tail expanding up to ~ 70. Each primary vertex is reconstructed using a subset of the tracks in the event; those tracks are said to be linked to that primary vertex.

1.1 Primary vertex from tracks

Each B_s^0 decay is reconstructed from 4 tracks and each track is linked to a primary vertex that can be used as B_s^0 creation point. This approach however does suffer from some problems: the first issue is the possibility of having tracks linked to the same SV but to different primary vertices and there is also the possibility of tracks linked to the wrong primary vertex in case of "bad" reconstruction.

The simplest way to estimate this effect is a count, for each SV, of the tracks linked to the same PV: the result is shown in **Table 4.1**.

Event Type	Number of events $\cdot 10^5$	Fraction
Total number of events	32.2	1
4 Tracks with same PV	23.5	0.728
3 Tracks with same PV	5.49	0.172
2 Tracks with same PV	3.02	0.094
No Tracks with same PV	0.18	0.006

Table 4.1: Number of events with tracks linked to the same primary vertex

In this case for the subsequent analysis only those events with at least 3 tracks linked to the same vertex, chosen as B_s^0 creation point, will be selected.

1.2 Primary vertex from pointing angle

A different approach to choose the primary vertex to use as creation point uses the tracks momenta instead of relying on their link with the PV.

The B_s^0 is electrically neutral so it is not deflected by the magnetic field, it's then possible to assume its trajectory as straight and having a direction identical to its momentum at the decay point; the momentum is then simply given by the vector sum of its decay product momenta:

$$\vec{p}_B = \sum_{i=1}^{4} \vec{p_i}$$

where $\vec{p_i}$ is the 3-dimensional momentum of the i-th track; in the reconstruction analysis the $\vec{p_i}$ momenta at the decay point have been estimated by extrapolating the track directions to the reconstructed secondary vertex position.

It's then possible to compare this vector with the $\vec{d_v}$ vector connecting a generic primary vertex with the SV of the event and compute the angle α, which is called "pointing angle", between the two; the selected PV will then be the one that minimizes this angle.

The distribution of the cosine of the pointing angle, shown in **Figure 4.1** shows that in most of the cases the primary vertex chosen with this method has a value of $\cos\alpha$ close to 1, which is the expected value in case of infinite precision on both the vertices position and momentum estimation; the peak at $\cos\alpha = -1$ is due to events where the SV is near the PV, leading to a large error on the $\vec{d_v}$ direction.

A quantitative description can be done by integrating in various ranges the number of events, as shown in **Table 4.2**.

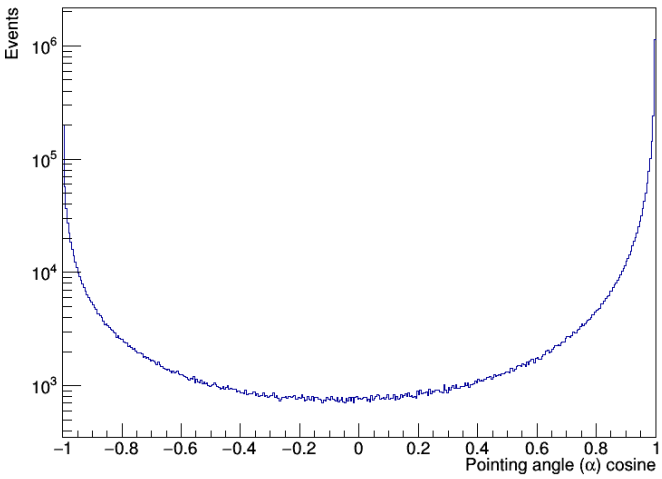

Figure 4.1: Cosine of the pointing angle α distribution in logarithmic scale

Range	Events ($\cdot 10^5$)	Fraction
Total events	32.2	1
$[0.95, 1]$	19.2	0.597
$[0.9, 0.95]$	2.2	0.068
$[0.8, 0.9]$	1.6	0.049
$[0.7, 0.8]$	0.7	0.022
$[-1, -0.95]$	4.3	0.132
$[-0.95, -0.9]$	0.8	0.024
$[-0.9, -0.8]$	0.7	0.023

Table 4.2: Number of events in $\cos\alpha$ ranges

1.3 Refitted Primary Vertices

During the estimation of the B_s^0 creation point, however chosen the PV, the possible presence of the decay products of the meson itself does change the estimated position of the vertex and, as a consequence, biases the estimation of the flight distance.

To estimate this bias, and possibly remove it, a primary vertex refit is done, starting from the vertex chosen with the pointing angle, after removing the tracks belonging to the B_s^0 decay products; the vertices thus obtained are called "refitted vertices".

The set of tracks used for the refitting process can be composed by all the tracks linked to that specific PV except the B_s^0 tracks or a subset of those tracks, selected from the Particle Flow algorithm[7] which selects the tracks comparing the response from many

detectors (tracker, calorimeter...).

During the refit process there is also the possibility of applying a constraint which requires the vertex to belong to the Beam Spot line; the combination of the different options results in 4 refitted primary vertices:

- All Tracks: refitted vertex with all the tracks excluding the B_s^0 ones, with Beam Spot constraint;
- All Tracks No BS: refitted vertex with all the tracks excluding the B_s^0 ones, without Beam Spot constraint;
- PF Only: refitted vertex with tracks selected from Particle Flow algorithm, excluding the B_s^0 ones, with Beam Spot constraint;
- PF No BS: refitted vertex with tracks selected from Particle Flow algorithm, excluding the B_s^0 ones, without Beam Spot constraint.

1.4 Primary vertices comparison

The procedures above described provide a set of 6 possible primary vertices that can be used as estimations of the creation point of the B_s^0.

The performance of the 6 choice criteria have been studied using a set of simulated events where the B_s^0 creation point is known. The distance alongside the z-axis was first studied: **Figure 4.2** shows the difference on z axis between the position of simulated creation point and the reconstructed PV position.

The total distribution was fitted using a probability density function (PDF) given by the sum of two gaussian with the same mean (μ):

$$M(x) = f_1 \cdot g_1(x) + (1 - f_1) g_2(x) \quad \text{with} \quad g_{12}(x) = \frac{1}{\sigma_{12}\sqrt{2\pi}} \exp\left[-\frac{1}{2}\left(\frac{x-\mu}{\sigma_{12}}\right)^2\right] \tag{4.1}$$

The total width σ of the probability density function is then computed starting from the two gaussian widths σ_{12}:

$$\sigma = \sqrt{f_1 \cdot \sigma_1^2 + (1 - f_1) \cdot \sigma_2^2} \pm \sqrt{\frac{(f_1\sigma_1\delta_1)^2 + ((1-f_1)\sigma_2\delta_2)^2 + (\sigma_1^2 - \sigma_2^2)^2\delta_f^2/2}{f_1 \cdot \sigma_1^2 + (1 - f_1) \cdot \sigma_2^2}} \tag{4.2}$$

where δ_{12} is the error associated to σ_{12} and δ_f is the error associated to the ratio of the two gaussian (f_1).

The fit results are shown in **Table 4.3**:

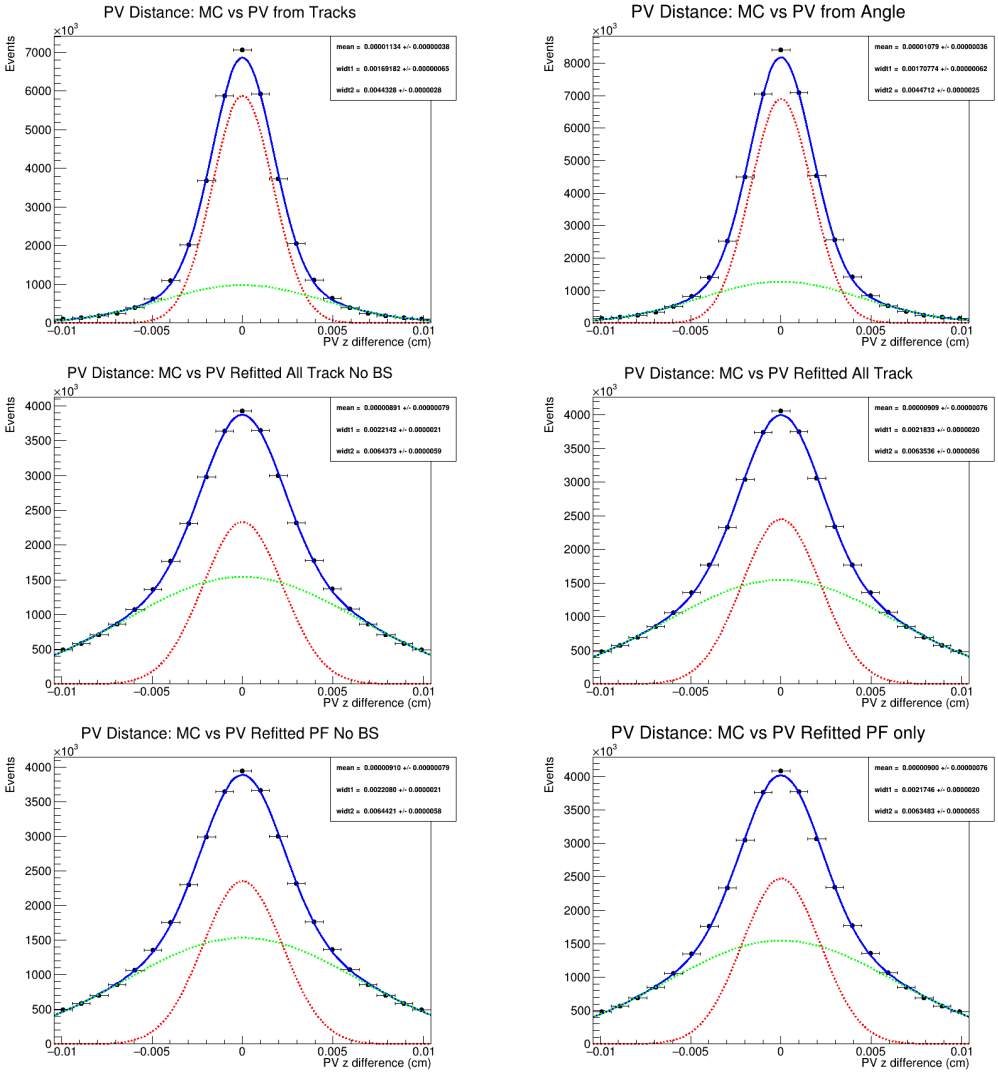

Figure 4.2: Difference on z axis between primary vertex from MC and reconstructed vertex

Both the plots and the table show that the refitted vertices have a slightly bigger dispersion and smaller offset but all of them can be considered good estimations of the actual creation point since the value of deviation and offset are respectively 1 and 3 order of magnitude smaller than the expected average flight distance of a B_s^0: $c\tau \sim 0.045$ cm.[6]

Vertex from:	$\mu(\cdot 10^{-5} cm)$	$\sigma_1(\cdot 10^{-3} cm)$	$\sigma_2(\cdot 10^{-3} cm)$	$\sigma(\cdot 10^{-3} cm)$
Tracks	1.130 ± 0.039	1.6918 ± 0.0007	4.432 ± 0.003	2.811 ± 0.002
Angle	1.075 ± 0.036	1.7076 ± 0.0006	4.471 ± 0.003	2.899 ± 0.002
All Tracks	0.906 ± 0.077	2.1832 ± 0.0020	6.354 ± 0.006	5.191 ± 0.005
All no BS	0.882 ± 0.080	2.2140 ± 0.0021	6.438 ± 0.006	5.291 ± 0.006
PF only	0.896 ± 0.077	2.1744 ± 0.0020	6.349 ± 0.006	5.180 ± 0.005
PF no BS	0.904 ± 0.080	2.2083 ± 0.0021	6.446 ± 0.006	5.287 ± 0.005

Table 4.3: Fit result from primary vertex z-difference distribution

2 Flight distance estimation

In order to estimate the mean lifetime of the B_s^0 meson it's important to properly calculate its flight distance; to get an higher resolution, position and momentum information are combined.

The flight distance, in the laboratory, is taken from the formula:

$$d^{Labo} = \frac{\vec{d_v} \cdot \vec{p}}{|\vec{p}|} = |\vec{d_v}| \cos\alpha$$

where $\vec{d_v}$ is the vector that connects primary to secondary vertex and α is the pointing angle defined in **Section 1.2** of this chapter.

In the particle rest frame the flight distance is obtained from the previous formula through relativistic correction:

$$d^{Rest} = ct = \frac{d^{Labo} \cdot m_B}{|\vec{p}|} = \frac{\vec{d_v} \cdot \vec{p} m_B}{p^2}$$

where t is the particle proper decay time and m_B is the particle mass.

The precision on the z coordinate is worse than on xy coordinates due to the detector properties, for this reason all the distances and momenta from the previous formulas are projected on the XY-plane leading to a more accurate estimation of ct:

$$d_{xy}^{Labo} = \frac{\vec{d}_{xy} \cdot \vec{p}_{xy}}{p_T} = |\vec{d}_{xy}| \cos\alpha_{xy}$$
$$d^{Rest} = ct = \frac{d_{xy}^{Labo} \cdot m_B}{p_T} = \frac{\vec{d}_{xy} \cdot \vec{p}_{xy} m_B}{p_T^2}$$

The possibility of choosing between 6 primary vertices gives as many estimation of the flight distance; using the same set of Monte Carlo data it's possible to compare the value of ct obtained from the reconstruction with the known value from the simulation.

The distribution was fitted using a PDF composed by 3 gaussian distribution ($g_{123}(x)$) with same mean and different deviation:

$$M(x) = f_1 \cdot g_1(x) + (1 - f_1)[f_2 \cdot g_2(x) + (1 - f_2)g_3(x)] \tag{4.3}$$

and the total width σ of the distribution is computed extending **Formula 4.2** to the new distribution.

In **Figure 4.4** the histogram of the difference between the simulated flight distance and the value obtained from each primary vertex is shown, whereas **Table 4.4** summarizes the fit result:

Vertex from:	$\mu(\cdot 10^{-5} cm)$	$\sigma_1(\cdot 10^{-3} cm)$	$\sigma_2(\cdot 10^{-3} cm)$	$\sigma_3(\cdot 10^{-3} cm)$	$\sigma(\cdot 10^{-3} cm)$
Tracks	5.39 ± 0.04	1.354 ± 0.002	2.368 ± 0.003	4.889 ± 0.007	3.274 ± 0.007
Angle	-4.42 ± 0.03	1.306 ± 0.002	2.292 ± 0.003	4.599 ± 0.007	3.062 ± 0.006
All Tracks	0.81 ± 0.03	1.348 ± 0.002	2.332 ± 0.003	4.940 ± 0.008	3.228 ± 0.006
All no BS	11.08 ± 0.05	1.373 ± 0.004	2.500 ± 0.004	5.648 ± 0.009	3.919 ± 0.009
PF only	0.90 ± 0.03	1.346 ± 0.002	2.327 ± 0.003	4.914 ± 0.008	3.214 ± 0.007
PF no BS	11.84 ± 0.05	1.368 ± 0.004	2.492 ± 0.004	5.612 ± 0.009	3.899 ± 0.009

Table 4.4: Fit result from flight distance difference distribution

Both the plots and the fit results show that the flight distances computed from all the choices of the primary vertex can be considered good estimations due to the value of mean and offset being more than one order of magnitude smaller than the flight distance itself; as best choice for the primary vertex the one obtained from the pointing angle minimization, which has the smallest distribution width, is taken.

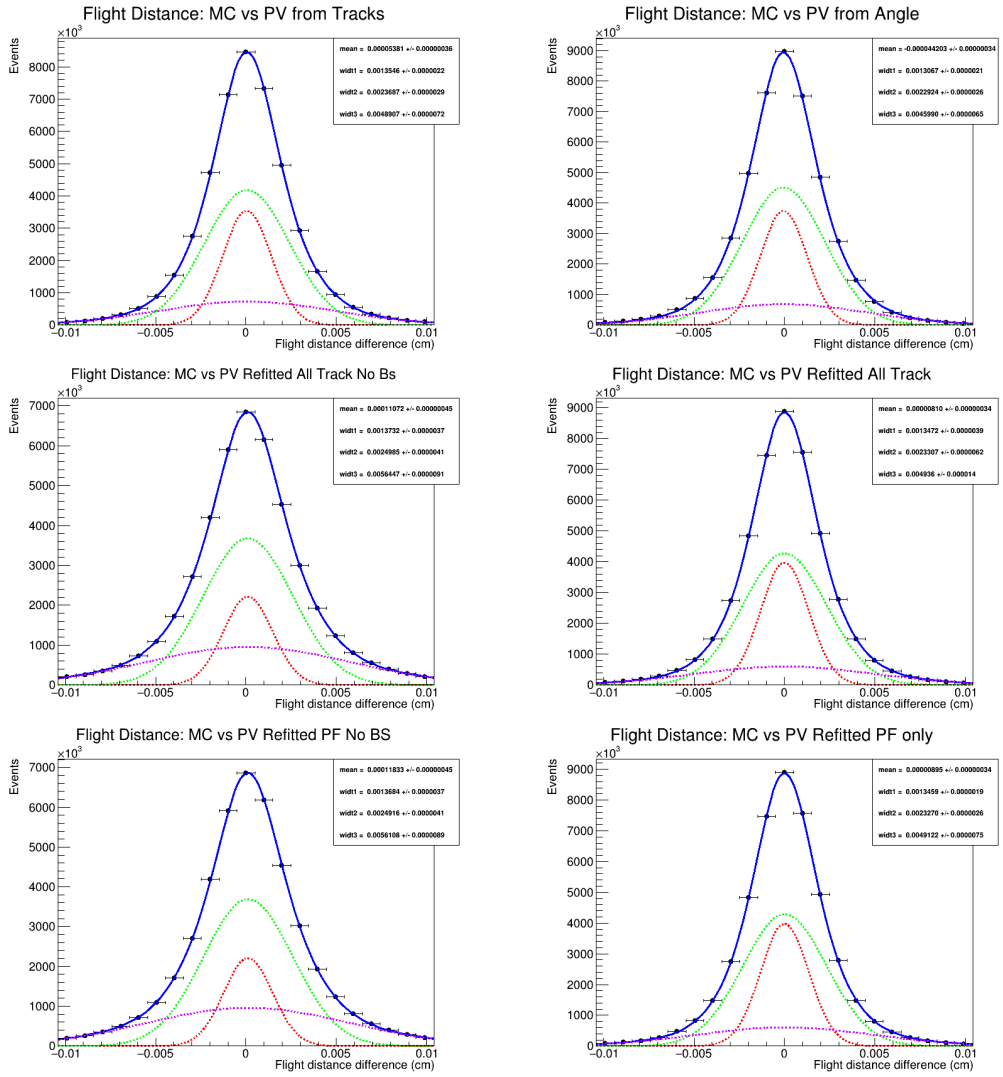

Figure 4.3: B_s^0 flight distance estimation difference between primary vertex from MC and reconstructed vertex

2.1 Data samples

The previous plots are obtained from a simulated data sample; once the PV is chosen the flight distance distribution, shown in **Figure 4.4**, can be studied:

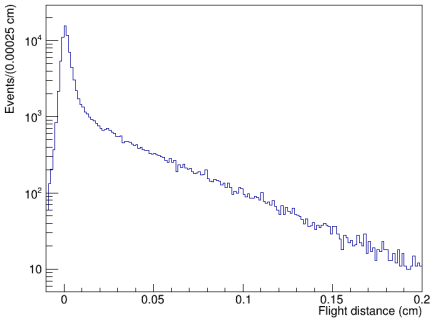

(a) "Inclusive" trigger

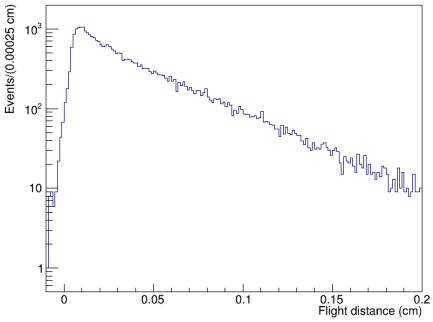

(b) "Displaced" trigger

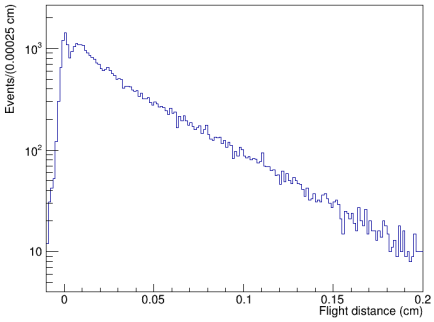

(c) "OR" trigger

Figure 4.4: B_s^0 flight distance obtained from different data samples with primary vertex chosen by pointing angle minimization

The plots clearly show that the request of the event being accepted by the "Displaced" trigger and its logic OR with the "Additional Muons" trigger reduce considerably the background level: the central peak visible in **Figure 4.4(a)** is mainly composed by background events which are rejected by the displacement request. On the other side, the effect of the displacement requirement in the trigger is clearly visible as a drop at small distance as shown in **Figure 4.4(b)** and **Figure 4.4(c)**.

Chapter 5

Lifetime Fit

The estimation of the B_s^0 mean lifetime is done through the use of a 2-dimensional fit with a PDF composed by the product of a distribution for the reconstructed mass and one for the flight distance; the PDF is fitted to the data with an unbinned maximum likelihood method using the RooFit tool[8] of the ROOT[9] system.

The 2-dimensional fit, due to large number of parameters, may become unstable; for this reason the fit is performed in several steps.

1 Mass analysis

In **Figure 3.4** the estimated mass on the reconstructed B_s^0 is shown, its distribution shows a central peak near the expected value of the reconstructed mass which is the signal, and a combinatorial background. This distribution has been fitted with the sum of two gaussians with a common mean, for the signal, and a second degree polynomial, for the background.

The background distribution was first fitted on the sidebands of the data sample, obtained by selecting only those B_s^0 with a reconstructed mass $m_B > 5.50$ GeV/c^2 and $m_B < 5.24$ GeV/c^2, as shown in **Figure 5.1**.

In the second step the full distribution of signal and background was fitted with the total PDF:

$$\mathcal{M}(m) = f_s \cdot [f_g \cdot g_1(m) + (1 - f_g)g_2(m)] + (1 - f_s)p_2(m) \tag{5.1}$$

where g_{12} are the two gaussian distributions, p_2 is the second degree polynomial, f_s is the fraction of signal events in the data set and f_g is the fraction between the two signal distributions: the result of this fit is shown in **Figure 5.2**.

In this fit the results of the first step (the background distribution coefficients) are kept fixed, allowing an easier convergence of the fit.

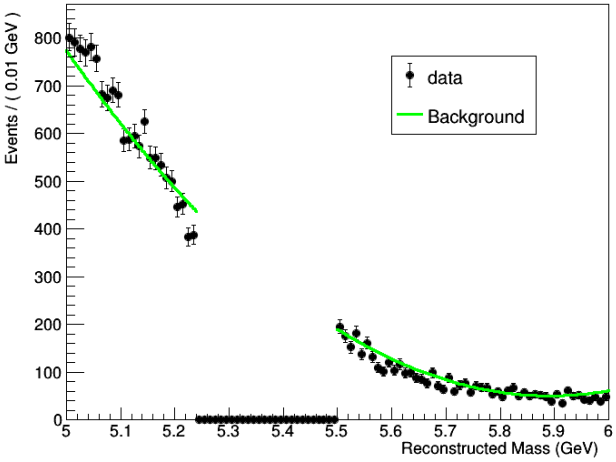

Figure 5.1: Polynomial fit of the B_s^0 reconstructed mass background events; events from "Displaced" trigger data samples

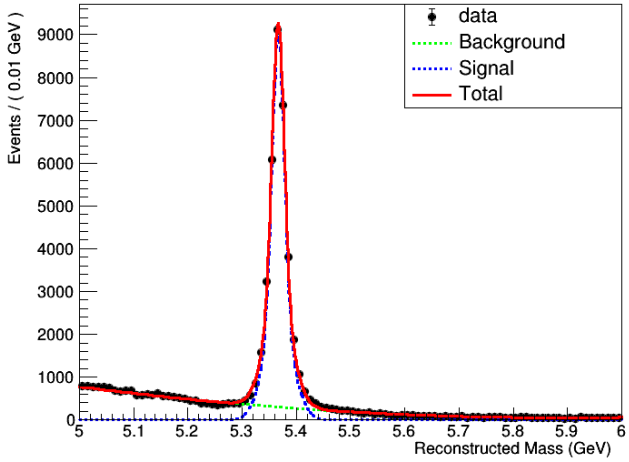

Figure 5.2: Full distribution fit of the B_s^0 reconstructed mass events; events from "Displaced" trigger data sample

The same PDF was used to fit the data samples obtained from the "Inclusive" and "OR" trigger, the corresponding results are shown in **Figure 5.3**.

The values of fitted B_s^0 mass, represented by the mean of the signal distribution, obtained from the 3 data samples, are shown in **Table 5.1**; the results obtained from all the data samples are in agreement with the world average value[6] of B_s^0 mass $m_{PDG} = 5.36688 \pm 0.00017$ GeV/c^2.

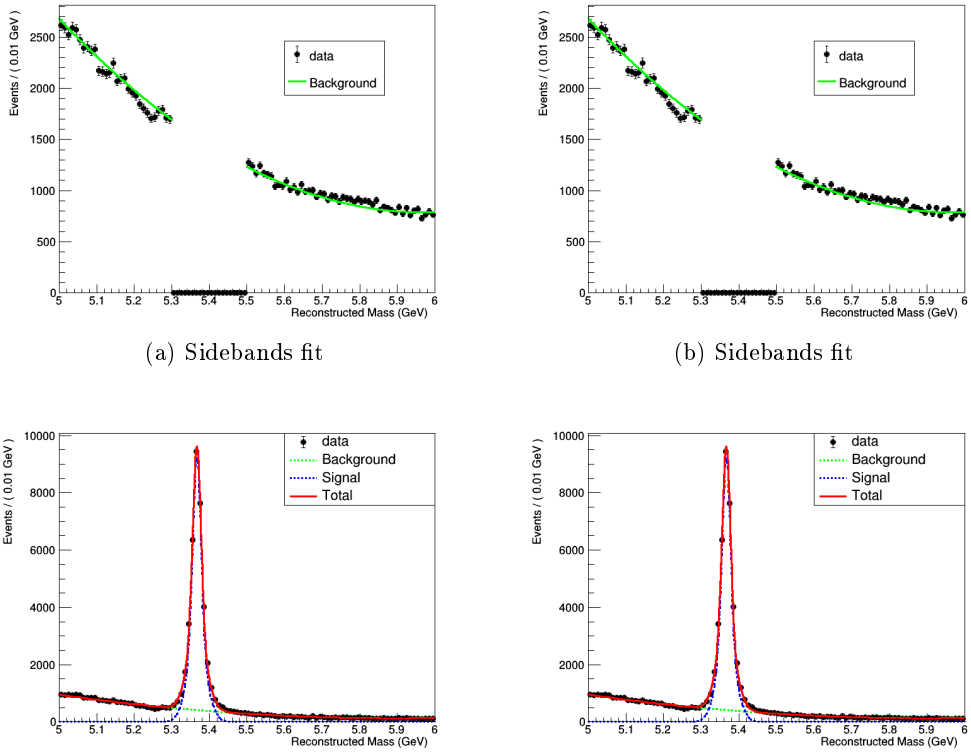

(a) Sidebands fit

(b) Sidebands fit

(c) Full distribution fit

(d) Full distribution fit

Figure 5.3: Fit of the reconstructed B_s^0 mass from different data samples: on the left events from the "Inclusive" data sample, on the right events from the "OR" trigger data sample

Selection	B_s^0 mass (GeV/c^2)
Inclusive trigger	5.36670 ± 0.00010
Displaced trigger	5.36664 ± 0.00010
OR trigger	5.36661 ± 0.00010

Table 5.1: B_s^0 reconstructed mass result from fit, statistical error only

2 Efficiency

The distribution of the reconstructed flight distance can be distorted due to the dependence of the reconstruction efficiency on the distance itself, part of this dependence is due to the trigger algorithm, especially for the displaced trigger.

The efficiency was estimated using the simulated events, comparing the flight distance distribution for the reconstructed decays and for the whole simulated distribution. Using the entries in each bin of the histograms it's possible to estimate the value of the efficiency ϵ as the ratio between the reconstructed decays number and the simulated one:

$$\epsilon = \frac{N_R}{N_S} \qquad \sigma_\epsilon = \sqrt{\frac{\epsilon(1-\epsilon)}{N_S}} \tag{5.2}$$

where σ_ϵ is the error associated to the efficiency value.

The measured efficiency in function of the flight distance was fitted with an exponential convoluted with a gaussian:

$$\mathcal{E}(d) = \lambda e^{-\lambda d} \otimes \frac{1}{\sigma\sqrt{2\pi}} \exp\left[-\frac{(d-\mu)^2}{2\sigma^2}\right] \tag{5.3}$$

The results obtained with the simulated events fulfilling the displaced trigger requirements are shown in **Figure 5.4**

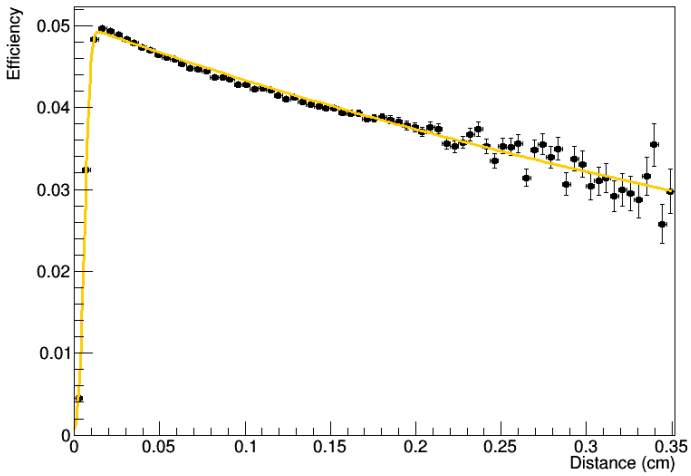

Figure 5.4: Efficiency dependence on the distance, simulated data sample with "Displaced" trigger requirement

The same function was used to fit the efficiency for the "OR" trigger data sample; for the "Inclusive" trigger data sample, which accepts a large number of events without a displacement requirement, a second degree polynomial distribution was used: the results shown in **Figure 5.5**

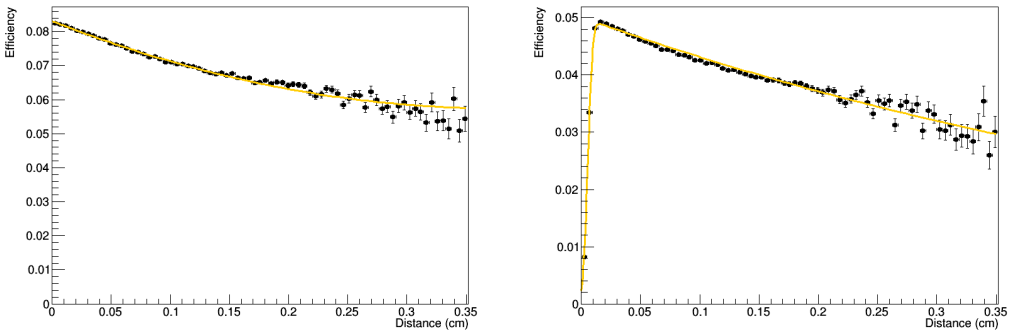

(a) "Inclusive" trigger (b) "Displaced" OR "Additional Muon" trigger

Figure 5.5: Efficiency dependence on the distance, simulated data sample with different trigger requirements

3 Flight distance analysis

3.1 Backgroung Fit

In the flight distance distribution the background is not clearly visible as in the reconstructed mass histogram, a data sample to study its distribution is built by selecting the events whose reconstructed mass belong to the sidebands of the histogram.

The distribution thus obtained was fitted with a PDF composed by two exponentials convoluted with a gaussian plus a gaussian centered in the origin; the two exponentials represent the combinatorial background while the convoluted gaussian allows to estimate the detector resolution:

$$\mathcal{B}(d) = f_p \cdot \exp\left[-\frac{(d-\mu_p)^2}{2\sigma_p^2}\right] + (1-f_p)\cdot\left[f_r \cdot e^{-\lambda_1 d} + (1-f_r)\cdot e^{-\lambda_2 d}\right] \otimes \exp\left[-\frac{(d-\mu_r)^2}{2\sigma_r^2}\right] \tag{5.4}$$

the centered gaussian mean (μ_p) may be imposed to be 0 or left free in the fit. The fit result on the "Displaced" trigger data sample is shown in **Figure 5.6**:

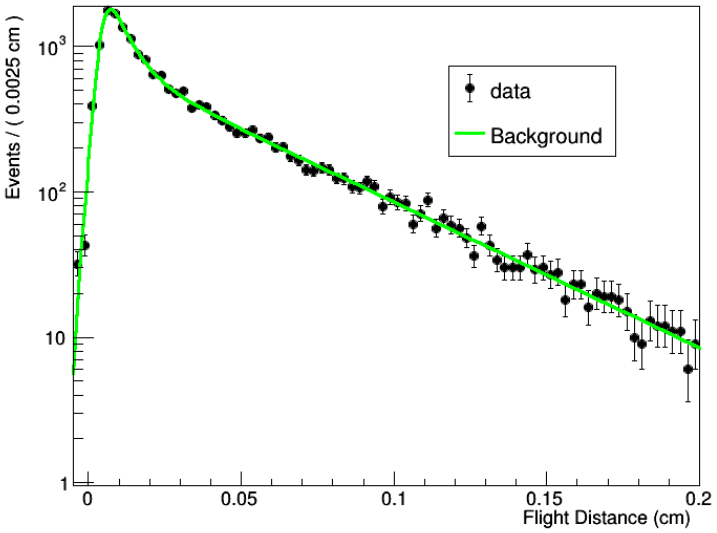

Figure 5.6: Background fit of the reconstructed B_s^0 flight distance, events from the "Displaced" trigger data sample, selected from the mass distribution sideband, PV obtained with the pointing angle minimization method

The same function was used to fit the flight distance background distribution obtained from the "OR" trigger data samples, giving the results shown is **Figure 5.7**.

The distribution obtained from the "Inclusive" trigger, which does not require a displacement, shows a central prompt and a left tail composed of background events, in order to fit this distribution a left-sided exponential convoluted with the gaussian resolution was added to the PDF and an additional step was added to the fit procedure: at first only the right side of the background distribution was fitted, the results thus obtained have then been used as initial values in the fit of the whole background distribution.

The fit results of both steps are shown in **Figure 5.8**:

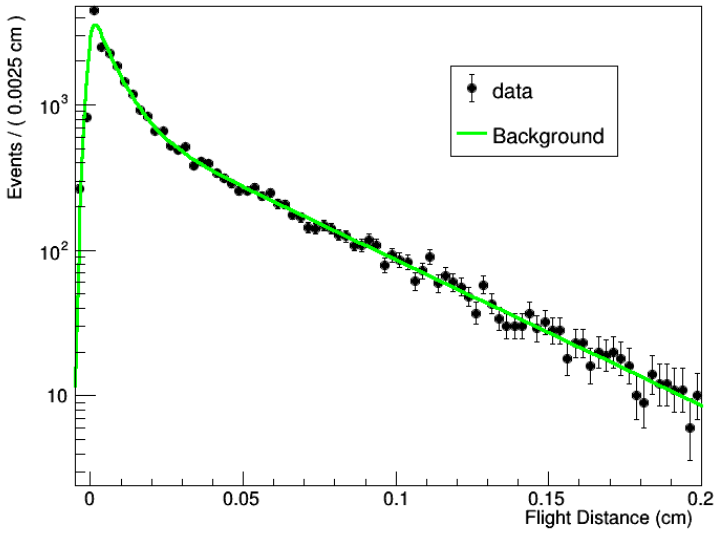

Figure 5.7: Background fit of the reconstructed B_s^0 flight distance, events from the "Displaced" OR "Additional Muon" trigger data sample, selected from the mass distribution sidebands, PV obtained with the pointing angle minimization method

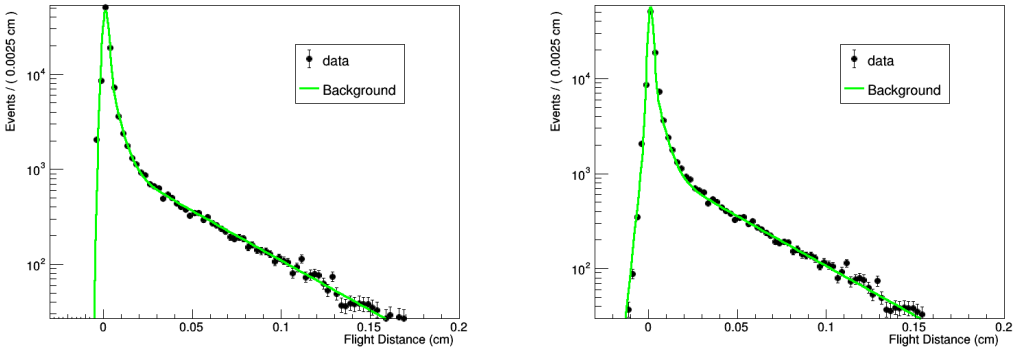

(a) First step: right side fit (b) Second step: total distribution fit

Figure 5.8: Background fit of the reconstructed B_s^0 flight distance, events from the "Inclusive" trigger data sample, selected from the mass distribution sidebands, PV obtained with the pointing angle minimization method

3.2 Total Fit

The last step of the fit procedure consists in the estimation of the B_s^0 lifetime.

In the previous analysis the parameters describing the reconstructed mass (**Formula 5.1**) and the flight distance background (**Formula 5.4**) have been obtained; the PDF describing the signal is composed by the product of an exponential representing the B_s^0 decay convoluted with the gaussian resolution (the same used for the background PDF) with the efficiency function described in **Formula 5.3**; the parameter of the signal exponential distribution will then be the estimated value of the B_s^0 lifetime.

The final fit is performed over the whole 2-dimensional distribution of reconstructed mass and flight distance, the PDF used to describe the data is:

$$\mathcal{F}(d,m) = \mathcal{M}(m) \cdot [f_s \cdot \mathcal{S}(d) \otimes \mathcal{R}(d) \cdot \mathcal{E}(d) + (1 - f_s)\mathcal{B}(d)] \tag{5.5}$$

where:

- $\mathcal{M}(m)$ is the reconstructed mass PDF described in **Formula 5.1**,
- $\mathcal{B}(d)$ is the background flight distance described in **Formula 5.4**,
- $\mathcal{E}(d)$ is the efficiency function described in **Formula 5.3**,
- $\mathcal{R}(d)$ is the gaussian PDF describing the detector resolution,
- $\mathcal{S}(d)$ is the exponential representing the B_s^0 decay: $\mathcal{S}(d) = e^{-\frac{d}{c\tau}}$,
- f_s quantifies the ratio between signal and background events.

The fit results for the "Displaced", "OR trigger" and "Inclusive" trigger data sample are respectively shown in **Figure 5.9**, **Figure 5.10**, **Figure 5.11**, where the PV chosen is the one obtained from the pointing angle minimization:

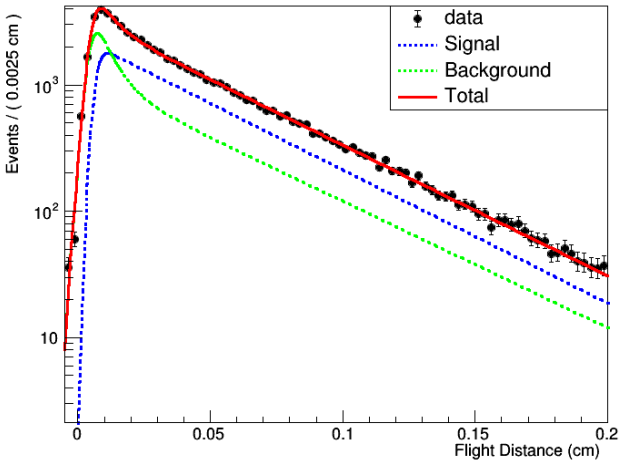

Figure 5.9: Fit of total B_s^0 flight distance distribution, events from "Displaced" trigger data sample

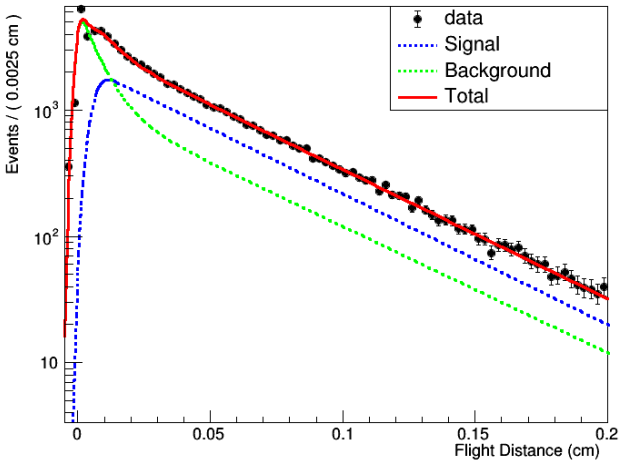

Figure 5.10: Fit of total B_s^0 flight distance distribution, events from "OR trigger" data sample

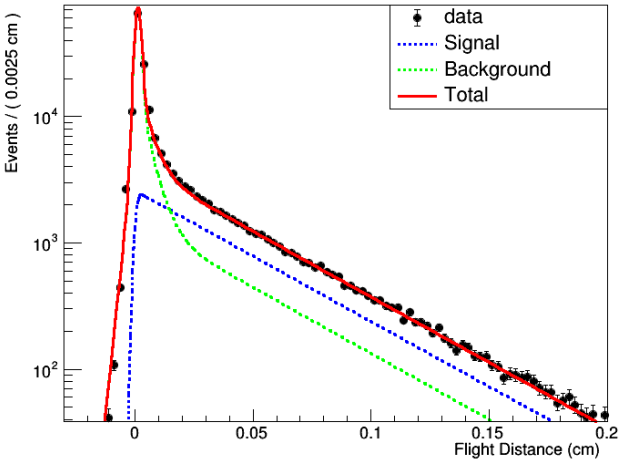

Figure 5.11: Fit of total B_s^0 flight distance distribution, events from "Inclusive" trigger data sample

4 Final results

When fitting the 2-dimensional PDF to the whole data distribution all the parameters obtained in the reconstructed mass and flight distance background fit have been kept constant to allow an easier convergence of the fit procedure.

To check the effect of this on the final fit result the fit procedure has been repeated leaving free in the final fit some of those parameter whose role is relevant also for the signal distribution:

- Variance of the resolution gaussian,
- Ratio between the centered gaussian and the combinatorial background,
- Mean of the centered gaussian.

In order to estimate the systematic error on of the B_s^0 lifetime measurement all the steps of the previous analysis have been repeated for each data sample using every choice of the primary vertex described in the **Chapter** 4 and with the possibility of keeping fixed or free the parameters above mentioned.

The results of the estimated B_s^0 mean lifetime for each possible combination of choices are shown in **Table 5.2**, **Table 5.3** and **Table 5.4**, where the number in the bracket gives the statistical error on the last digit.

The mean flight distance, from the fit, in the "Displaced" trigger data sample, choosing the "angle" primary vertex and leaving free all the parameters listed above is $c\tau = 0.0434 \pm 0.0003$ cm where only the statistical error is quoted; this value corresponds to a mean lifetime of $\tau = 1.448 \pm 0.010$ ps, the world average B_s^0 lifetime is $\tau = 1.510 \pm 0.004$ ps.

The systematic uncertainty coming from the PV choice can be estimated as $\delta_{c\tau} \sim 0.0003$ cm; more important effects are seen from the choice of the trigger, through the efficiency estimation and the fit procedure.

Settings			Primary vertex from:					
Mean	Frac	Reso	All tracks no BS	All tracks	Angle	PF Only	PF no BS	Tracks
Free	Free	Free	0.0436(3)	0.0430(3)	0.0431(3)	0.0436(3)	0.0430(3)	0.0429(3)
Free	Free	Fixed	0.0433(3)	0.0428(3)	0.0427(3)	0.0433(3)	0.0428(3)	0.0428(3)
Free	Fixed	Free	0.0433(3)	0.0430(3)	0.0425(3)	0.0433(3)	0.0430(3)	0.0429(3)
Free	Fixed	Fixed	0.0434(3)	0.0429(3)	0.0429(3)	0.0437(3)	0.0429(3)	0.0428(3)
Fixed	Free	Free	0.0432(3)	0.0428(3)	0.0425(2)	0.0432(3)	0.0428(3)	0.0428(3)
Fixed	Free	Fixed	0.0433(3)	0.0429(3)	0.0429(3)	0.0435(3)	0.0429(3)	0.0428(3)
Fixed	Fixed	Free	0.0434(3)	0.0430(3)	0.0429(3)	0.0434(3)	0.0430(3)	0.0428(3)
Fixed	Fixed	Fixed	0.0434(3)	0.0429(3)	0.0429(3)	0.0434(3)	0.0429(3)	0.0428(3)

Table 5.2: Estimated B_s^0 lifetime, events from "Inclusive" trigger data sample

Settings			Primary vertex from:					
Mean	Frac	Reso	All tracks no BS	All tracks	Angle	PF Only	PF no BS	Tracks
Free	Free	Free	0.0437(3)	0.0432(3)	0.0434(3)	0.0436(3)	0.0432(3)	0.0431(3)
Free	Free	Fixed	0.0437(3)	0.0432(3)	0.0434(3)	0.0436(3)	0.0432(3)	0.0431(3)
Free	Fixed	Free	0.0443(3)	0.0440(3)	0.0439(3)	0.0442(3)	0.0434(3)	0.0439(3)
Free	Fixed	Fixed	0.0437(3)	0.0432(3)	0.0434(3)	0.0436(3)	0.0432(3)	0.0431(3)
Fixed	Free	Free	0.0443(3)	0.0434(3)	0.0439(3)	0.0443(3)	0.0440(3)	0.0439(3)
Fixed	Free	Fixed	0.0437(3)	0.0432(3)	0.0434(3)	0.0436(3)	0.0432(3)	0.0431(3)
Fixed	Fixed	Free	0.0443(3)	0.0440(3)	0.0439(3)	0.0443(3)	0.0434(3)	0.0439(3)
Fixed	Fixed	Fixed	0.0443(3)	0.0440(3)	0.0439(3)	0.0444(3)	0.0440(3)	0.0439(3)

Table 5.3: Estimated B_s^0 lifetime, events from "Displaced" trigger data sample

Settings			Primary vertex from:					
Mean	Frac	Reso	All tracks no BS	All tracks	Angle	PF Only	PF no BS	Tracks
Free	Free	Free	0.0441(3)	0.0441(3)	0.0446(3)	0.0441(3)	0.0441(3)	0.0440(3)
Free	Free	Fixed	0.0451(3)	0.0443(3)	0.0447(3)	0.0451(3)	0.0443(3)	0.0441(3)
Free	Fixed	Free	0.0441(3)	0.0441(3)	0.0446(3)	0.0441(3)	0.0441(3)	0.0440(3)
Free	Fixed	Fixed	0.0441(3)	0.0441(3)	0.0446(3)	0.0441(3)	0.0441(3)	0.0440(3)
Fixed	Free	Free	0.0451(3)	0.0442(3)	0.0447(3)	0.0451(3)	0.0443(3)	0.0441(3)
Fixed	Free	Fixed	0.0441(3)	0.0441(3)	0.0446(3)	0.0441(3)	0.0441(3)	0.0440(3)
Fixed	Fixed	Free	0.0451(3)	0.0443(3)	0.0447(3)	0.0451(3)	0.0443(3)	0.0441(3)
Fixed	Fixed	Fixed	0.0451(3)	0.0443(3)	0.0447(3)	0.0451(3)	0.0443(3)	0.0441(3)

Table 5.4: Estimated B_s^0 lifetime, events from "Displaced" OR "Additional Muon" trigger data sample

Chapter 6

Conclusions

The analysis has shown that the best assumption as creation point for the B_s^0 analysis is the primary vertex obtained from the pointing angle minimization, as shown in **Table 4.4**, due to its smaller dispersion when compared to the other candidates.

The B_s^0 meson mean lifetime can be obtained with good results through the fit procedure described in **Chapter** 5; performing several steps in the fitting process allows an easy convergence of the fit itself for high statistic data samples despite the use of many parameters is the Probability Density Function definition.

The result obtained from the "Displaced" trigger data sample fit with free parameters and the primary vertex chosen from the pointing angle minimization is: $\tau = 1.448 \pm 0.010$ps; the systematic error associated with the primary vertex choice has an one percent order of magnitude.

Bibliography

[1] CMS Collaboration. "Measurement of the CP-violating weak phase ϕ_s and the decay width difference $\Delta\Gamma_s$ using the $B_s^0 \to J/\psi\phi(1020)$ decay channel in pp collisions at $s = 8$ TeV". In: *Phys. Lett. B* 757 (2016). 97. DOI: 10.1016/j.physletb.2016.03.046.

[2] Torbjörn Sjöstrand. "A Brief Introduction to PYTHIA 8.1". In: *CompPhys Comm.* 178 (2008). 852. DOI: 10.1016/j.cpc.2008.01.036.

[3] D. Lange. "The EvtGen particle decay simulation package". In: *Nucl. Inst. and Methods in Phys. Res.* A NIM A 462 (2001). 152. DOI: 10.1016/S0168-9002(01)00089-4.

[4] CMS Collaboration. "The CMS experiment at the CERN LHC". In: *JINST* 3 (2008). S08004. DOI: 10.1088/1748-0221/3/08/s08004.

[5] CMS Collaboration. "The CMS trigger system". In: *JINST* 12 (2017). P01020. DOI: 10.1088/1748-0221/12/01/P01020.

[6] Tanabashi et al. (Particle Data Group). "Review of Particle Physics". In: *Phys. Rev. D* 98 (2018). 030001. DOI: 10.1103/PhysRevD.98.030001.

[7] CMS Collaboration. "Particle-flow reconstruction and global event description with the CMS detector". In: *JINST* 12 (2017). P10003. DOI: 10.1088/1748-0221/12/10/P10003.

[8] *The RooFit Toolkit for Data Modeling*. URL: http://roofit.sourceforge.net/intro.html.

[9] R. Brun and F. Rademakers. "ROOT - An Object Oriented Data Analysis Framework". In: *Nucl. Inst. and Methods in Phys. Res. A* 389 (1997). 81. DOI: 10.1016/S0168-9002(97)00048-X.